1 Title page

Title

Full-length Dhh and N-terminal Shh act as competitive antagonists to regulate angiogenesis and vascular permeability

Short title

FL-Dhh and N- Shh are competitive antagonists

Authors and affiliations

Pierre-Louis Hollier[1*], Candice Chapouly[1*], Aissata Diop[1], Sarah Guimbal[1], Lauriane Cornuault[1], Alain-Pierre Gadeau[1] and Marie-Ange Renault[1]

* These authors contributed equally to this work

[1] Univ. Bordeaux, Inserm, Biology of Cardiovascular Diseases, U1034, F-33604 Pessac, France

Contact Info

Marie-Ange Renault
Inserm U1034
1, avenue de Magellan
33604 Pessac
France
e-mail : marie-ange.renault@inserm.fr
Tel : (33) 5 57 89 19 79

Category: Original Article

Total word count: 8354

2. Abstract

The therapeutic potential of Hedgehog (Hh) signalling agonists for vascular diseases is of growing interest. However, molecular and cellular mechanisms underlying the role of the Hh signalling in vascular biology remain poorly understood. **Aims:** The purpose of the present paper is to clarify some conflicting literature data. **Methods and Results**: With this goal we have demonstrated that, unexpectedly, ectopically administered N-terminal Sonic Hedgehog (N-Shh) and endogenous endothelial-derived Desert Hedgehog (Dhh) induce opposite effects in endothelial cells (ECs). Notably, endothelial Dhh acts under its full-length soluble form (FL-Dhh) and activates Smoothened in ECs, while N-Shh inhibits it. At molecular level, N-Shh prevents FL-Dhh binding to Patched-1 demonstrating that N-Shh acts as competitive antagonist to FL-Dhh. Besides, we found that even though FL-Hh ligands and N-Hh ligands all bind Patched-1, they induce distinct Patched-1 localization. Finally, we confirmed that in a pathophysiological setting i.e. brain inflammation, astrocyte-derived N-Shh act as a FL-Dhh antagonist. **Conclusion:** The present study highlights for the first time that FL-Dhh and N-Hh ligands have antagonistic properties especially in ECs. **Translational Perspective:** As a consequence, Hh ligands or forms of Hh ligands cannot be used instead of another for therapeutic purposes**.**

Keywords
Hedgehog signalling, Endothelium, Permeability, Antagonism, Multiple sclerosis

3. Introduction

Evidences accumulated over the past decades, identified Hedgehog (Hh) signalling as a new regulator of vascular homeostasis. More specifically, it has been shown to regulate both angiogenesis [1] and micro-vessel integrity [2]. Indeed, previous investigations have reported that antibody-mediated neutralization of Hh protein impairs ischaemia-induced angiogenesis both in the setting of hindlimb ischaemia and myocardial infarction in mice [3,4]. Accordingly, when Sonic Hedgehog (Shh), one of the Hh ligands, was administered either as a recombinant protein or via gene therapy, it enhanced the neovascularization of ischemic tissues by promoting both angiogenesis [1] and endothelial progenitor cell recruitment [5]. Besides, Hh signalling was shown to promote blood-brain barrier (BBB) integrity and immune quiescence in the setting of multiple sclerosis [2] and in the setting of stroke [6]. Additionally we have shown that disruption of Hh signalling specifically in ECs induces blood-nerve barrier breakdown and peripheral nerve inflammation [7]. As a consequence, the therapeutic potential of Hh signalling agonists for vascular diseases is of growing interest [8 9 10 11 12 13]. However, molecular and cellular mechanisms underlying the role of the Hh ligands in vascular biology remain poorly understood and conflicting results have been reported [14]. For Instance, while, as described above, most studies agree upon the proangiogenic role of Shh [1,5,15], unexpectedly, ischaemia-induced angiogenesis was shown to be accelerated in Shh-deficient mice [16]. Similarly, while Hh signalling is typically believed to promote endothelial barrier integrity [2,17], Glioblastoma-derived Desert Hedgehog (Dhh) was shown to disrupt the BBB [18]. Additionally, an early study reported that ectopic Shh overexpression in the dorsal neural tube induces haemorrhage in the spinal cord [19].

The Hedgehog (Hh) family of morphogens, which was identified nearly 4 decades ago in drosophila as crucial regulators of cell fate determination during embryogenesis, includes three members: Shh, Indian hedgehog (Ihh) and Dhh [20]. The interaction of Hh proteins with their specific receptor Patched-1 (Ptch1) de-represses the transmembrane protein Smoothened (Smo), which activates downstream pathways, including the Hh canonical pathway leading to the activation of Gli family zinc finger (Gli) transcription factors and so-called Hh non canonical pathways, which are independent of Smo and/or Gli [21]. However, while Shh, Ihh and Dhh, all bind to the same receptor, Ptch1, with close affinities, their ability to activate Gli-dependent transcription in fibroblast cell lines is dramatically different. Ihh is 6 times less potent than Shh, and Dhh is more than 10 times less potent than Ihh [22]. This has been one of the reasons why Shh is the main Hh gene considered for therapy. In contrast, some of Hh biological effects including Islet-1 induction [22] or activation of RhoA in ECs are equally induced by the 3 proteins [23].

Besides, Shh is synthesized as a pre-protein whose signal sequence is first cleaved to produce a full-length unmodified form. Then an autocatalytic reaction removes the carboxy-terminal domain and attaches a cholesterol moiety to the newly exposed carboxy-terminus. Shh is further modified by Hedgehog acyltransferase (Hhat) which catalyses the addition of a palmitate to the amino-terminus [24], to generate the Shh active form (N-Shh). Secretion and solubility of cholesterol-modified Shh depend on the transmembrane protein Disp1 (dispatched RND transporter family member 1) and the cell surface protein Scube2 (signal peptide, CUB domain and EGF like domain containing 2) [25]. Both Disp1 and Scube2 bind the cholesterol-anchor of Shh. On the contrary to Shh, Ihh and Dhh processing have been poorly investigated, and may differ. Indeed, Dhh is suggested not to undergo efficient autocatalytic cleavage [26].

The purpose of the present paper is to compare the vascular effects of endothelial-derived Dhh with those of ectopically administered N-Shh in order to determine whether Hh ligands rather promote

vessel integrity and quiescence or destabilize vessels to promote angiogenesis and to validate some debated vascular effects of Hh ligands. Notably, Shh is not expressed by ECs. ECs mainly express Dhh [17,27]. Ihh may be found in some vascular bed including the one of the eye choroid [28,29].

4. Methods

The data underlying this article are available in the article and in its online supplementary material.

4.1. Mice

Dhh Floxed (Dhh^{Flox}) mice were generated at the "Institut Clinique de la Souris" through the International Mouse Phenotyping Consortium (IMPC) from a vector generated by the European conditional mice mutagenesis program, EUCOMM and described before [17]. Shh Floxed (Shh^{Flox}) mice [30], Smo Floxed (Smo^{Flox}) mice [31], Tg(Slc1a3-cre/ERT)1Nat/J (Glast-Cre^{ERT2}) mice [32] and *Gt(ROSA)26Sor*$^{tm4(ACTB-tdTomato,-EGFP)Luo}$/J ($Rosa26^{mTmG}$) mice [33] were obtained from Jackson Laboratories. Tg(Cdh5-cre/ERT2)1Rha (Cdh5-CreERT2) mice [34] were a gift from RH. Adams.

Animal experiments were performed in accordance with the guidelines from Directive 2010/63/EU of the European Parliament on the protection of animals used for scientific purposes and approved by the local Animal Care and Use Committee of Bordeaux University (CEEA 50).

The Cre recombinase in Cdh5-Cre^{ERT2} mice was activated by intraperitoneal injection of 1 mg tamoxifen for 5 consecutive days at 8 weeks of age. Mice were phenotyped 2 weeks later. Successful and specific activation of the Cre recombinase has been verified before [27,35]. The Cre recombinase in Glast-Cre^{ERT2} mice was activated by intraperitoneal injection of 1 mg tamoxifen, twice a day for 5 consecutive days at 8 weeks of age. Mice were phenotyped 2 weeks later. Successful and specific activation of the Cre recombinase has been verified (Supplemental Figure 9A).

Both males and females were used in equal proportions except otherwise stated. Mice were sacrificed by cervical dislocation or pentobarbital overdose (300 mg/kg).

4.2. Mouse corneal angiogenesis assay

Pellets were prepared as previously described [36]. Briefly, either 5 µg of VEGFA (Shenandoah biotechnology) or rec N-Shh (Shenandoah biotechnology) diluted in 10 µL sterile phosphate-buffered saline (PBS) was mixed with 2.5 mg sucrose octasulfate-aluminum complex (Sigma-Aldrich Co., St. Louis, MO, USA), and 10 µL of 12% hydron in ethanol was added. The suspension was deposited on a 400-µm nylon mesh (Sefar America Inc., Depew, NY, USA), and both sides of the mesh were covered with a thin layer of hydron and allowed to dry.

Female mice were anaesthetized with an intraperitoneal (IP) injection of ketamine 100 mg/kg and xylazine 10 mg/kg. The eyes of the mice were topically anaesthetized with 0.5% Proparacaine™. The globe of the eye was proptosed with jeweler's forceps taking care to not damage the limbus vessel surrounding the base of the globe. Sterile saline was also be applied directly to each eye as needed during the procedure to prevent excessive drying of the cornea and to facilitate insertion of the pellet into the lamellar pocket of the eyes. Using an operating microscope, a central, intrasomal linear keratotomy was performed with a surgical blade parallel to the insertion of the lateral rectus muscle. Using a modified von Greafe knife, a lamellar micro pocket was made toward the temporal limbus by rocking the von Greafe knife back and forth. The pellet was placed on the cornea surface with jeweler's forceps at the opening of the lamellar pocket. A drop of saline was applied directly to the pellet, and using the modified von Greafe knife, the pellet was gently advanced to the temporal

end of the pocket. To avoid any pain, Buprenorphine was given at a dose of 0.05 mg/kg subcutaneously on the day of surgery.
Nine days after pellet implantation, mice were sacrificed, and eyes were harvested and fixed with 2% formalin. Capillaries were stained with rat anti-mouse CD31 antibodies (BMA Biomedicals, Cat#T-2001), and primary antibodies were visualized with Alexa 568–conjugated anti-rat antibodies (Invitrogen). Pictures were taken under 50x magnification. Angiogenesis was quantified as the CD31+ surface area using Image J software.

4.3. Central nervous system microinjection:

To obtain LV-N-Shh, pIRES-N-Shh [16] was digested by *NheI* and *HpaI*, the mouse N-Shh sequence was then cloned in pRRLsin.MND.MCS.WPRE (Addgene) that had been previously digested by *NheI* and *PmlI*. Lentviral particles were produced at the vectorology facility of Bordeaux University.
Mice (male and female used in equal proportion) were anaesthetized by 3% isoflurane inhalation and placed into a stereotactic frame (Stoelting, Illinois, USA). To prevent eye dryness, an ophthalmic ointment was applied at the ocular surface to maintain eye hydration during the time of surgery. The skull was shaved and the skin incised on 1 cm to expose the skull cap. Then, a hole was drilled into the skull above the cerebral cortex and 3 µL of an AdIL-1 [37], AdDL70 control (AdCtrl), LV-NShh or LV-GFP control (10^7 pfu) solution were microinjected at y=1 mm caudal to Bregma, x=2 mm, z=1.5 mm using a Hamilton syringe, into the cerebral cortex and infused for 3 minutes before removing the needle from the skull hole [38]. To avoid any pain, mice received a subcutaneous injection of buprenorphine (0.05 mg/kg) 30 minutes before surgery and again 8 hours post-surgery to assure a constant analgesia during the procedure and postoperatively. Mice were sacrificed by pentobarbital overdose. Those injected with the adenovirus were sacrificed 7 days post-surgery and those injected with the lentivirus were sacrificed 14 days post-surgery to maximize the vector effectiveness. For histological assessment, brains were harvested and fixed with 10% formalin for 3 hours before being incubated in 30% sucrose overnight and embedded in OCT. For each brain, the lesion area, identified by the puncture site, was cut into 7 µm thick sections.

4.4. Experimental autoimmune encephalomyelitis (EAE)

Ten week old female mice were immunized by subcutaneous injection of 300 µg myelin oligodendrocyte glycoprotein-35-55 (MOG35–55) (Hooke laboratories) in 200-µl Freund's adjuvant containing 300 µg/mL mycobacterium tuberculosis H37Ra (Hooke laboratories) in the dorsum. Mice were then administered with 500 ng pertussis toxin (PTX) IP on day of sensitization and 1 day later (Hooke laboratories). To avoid any pain, injections were performed under anaesthesia (3% isoflurane inhalation). Disease was scored (0, no symptoms; 1, floppy tail; 2, hind limb weakness (paraparesis); 3, hind limb paralysis (paraplegia); 4, fore- and hind limb paralysis; 5, death) [37] from day 7 post immunization until day 32 post immunization. At day 32, all the animals were euthanized by pentobarbital overdose. For histological assessment, cervical, lumbar and dorsal sections of each animal spinal cord, as well as the spleen, were harvested and fixed in formalin for 3 hours before being incubated in 30% sucrose overnight, embedded in OCT and cut into 7 µm thick sections.

4.5. Immunostaining

Prior to staining, brains were fixed with 10% formalin for 3 hours, incubated in 30% sucrose overnight, OCT embedded and cut into 7 µm thick sections. Cultured cells were fixed with 10% formaline for 10 minutes.

Human Cdh5 was stained using mouse anti-human Cdh5 antibodies (Santa Cruz Biotechnology, Inc, Cat#sc-9989). Mouse Cdh5 was stained using goat anti-mouse Cdh5 antibodies (R&D systems, Cat# AF1002). Cldn5 was stained using either mouse monoclonal anti-Cldn5 antibodies (Invitrogen, Cat# 35-2500) or rabbit polyclonal anti-Cldn5 antibodies (Invitrogen, Cat# 34-1600). Albumin and fibrinogen were stained using sheep anti-albumin antibodies (Abcam, Cat# ab8940) and rabbit anti-fibrinogen antibodies (Dako, Cat#A0080) respectively.
Leucocytes were identified using rat anti-mouse CD45 antibodies (BD Pharmingen Inc, Cat# 550539). Iba1+ microglia was identified using rabbit anti-Iba1 antibodies (FUJUFILM Wako chemicals, cat#019-19741). Reactive astrocytes were stained using rabbit anti-Gfap antibodies (ThermoFisher, Cat# OPA1-06100). Myelin was identified using rat anti-Mbp antibodies (Abcam, Cat# ab7349).
Hh ligands were stained using rabbit anti-Shh antibodies (Santa Cruz Biotechnology, Inc, Cat# sc-9024). Dhh was specifically stained using mouse anti-Dhh antibodies (Santa Cruz Biotechnology, Inc, Cat# sc-271168). Ptch1 was stained using rabbit anti-Ptch1 antibodies (Abcam, Cat# ab53715).
For immunofluorescence analyses, primary antibodies were resolved with Alexa Fluor®–conjugated secondary polyclonal antibodies (Invitrogen, Cat# A-21206, A-21208, A-11077, A-11057, A-31573, A-10037) and nuclei were counterstained with DAPI (1/5000). For both immunohistochemical and immunofluorescence analyses, negative controls using secondary antibodies only were done to check for antibody specificity.
BBB permeability was evaluated by measuring tight junction integrity and plasmatic protein extravasation. For each brain or spinal cord section, Cldn5+, Cdh5+, Fibrinogen+, and Albumin+ and IgG+ areas were quantified in 20 pictures taken at the margins of the lesion area under 40x magnification. CD45+ leukocytes were counted in 20 pictures randomly taken under 40x magnification. Gfap+ and NeuN+ areas were quantified in 10 pictures taken in and around the lesion area under 20X magnification. One section, localized in the Il1β-induced inflammatory lesion area, per brain was quantified for each mouse. Three sections/spinal cord was quantified (one cervical, one lumbar and one dorsal) for each mice to get a global vision of the inflammatory lesion.

4.6. Isolation of primary cultured mouse brain ECs

Mice were sacrificed by cervical dislocation. Brain was then harvested and cerebellum, olfactory bulb and white matter removed with sterile forceps. Additionally, meninges were eliminated by rolling a sterile cotton swab at the surface of the cortex. The cortex was then transferred in a potter containing 2 mL HBSS 1X w/o phenol red containing 10 mol/L HEPES and 0,1% BSA and the brain tissue was pounded to obtain an homogenate which was collected in a 15 mL tube. Cold 30% dextran solution was then added to the tube (V/V) to obtain a 15% dextran working solution. After a 25 min centrifugation at 3000 g at 4°C, the pellet (neurovascular components and red cells) was collected and the supernatant (dextran solution and neural components) was centrifuged again to get the residual vessels. Neurovascular components were then pooled and washed three time with HBSS 1X Ca^{2+}/Mg^{2+} free containing phenol red, 10 mmol/L HEPES and 0,1% BSA. The pellet was then suspended in DMEM containing 2 mg/mL collagenase/dispase (Roche), 0,147 µg/mL TLCK (Lonza) and 10 µg/mL DNAse 1 (Roche), pre-warmed at 37 °C, before being placed on a shaking table at maximum speed agitation at 37°C. After 30 min, the digestion was stopped by adding 10 mL HBSS 1X Ca^{2+}/Mg^{2+} free containing phenol red, 10 mmol/L HEPES and 0,1% BSA and washed again 3 times in this same buffer. The digested neurovascular pellet was finally re-suspended in mouse brain endothelial cell culture medium (DMEM 1 g/L glucose containing 20% FBS, 2% sodium pyruvate, 2% non-essential amino acids, 1 ng/mL FGF2 and 10 mg/mL gentamycin) and plated on dishes previously

coated with 2% Matrigel™ (BD biosciences). In each experiment, replicates were always prepared from independent animals (1 mice = one cell culture well).

4.7. Cell culture

Cell culture assays are described in the supplemental method section.

4.8. Statistics

Results are reported as mean ± SEM. Comparisons between groups were analysed for significance with the non-parametric Mann-Whitney test or a Kruskal-Wallis test followed by Dunn's multiple comparison test (for more than two groups) using GraphPad Prism v8.0.2 (GraphPad Inc, San Diego, Calif). Differences between groups were considered significant when $p \leq 0.05$ (*: $p \leq 0.05$; **: $p \leq 0.01$; ***: $p \leq 0.001$).

5. Results

5.1. Ectopic administration of N-Shh promotes angiogenesis while endothelial Dhh inhibits it.

Since Hh ligands are well known for their pro-angiogenic effect [1], we first used the mouse corneal angiogenesis model to compare the effect of ectopically administered recombinant N-Shh (rec N-Shh) and endogenous endothelial Dhh on angiogenesis. Consistent with previous investigations [1,15], implantation of N-Shh-containing pellets in the cornea of wild-type mice induced angiogenesis (Figure 1A-B). However, when VEGFA-containing pellets were implanted in the corneas of both EC specific Dhh knockout mice (Dhh^{ECKO}) and their control littermates, angiogenesis was significantly enhanced in Dhh^{ECKO} mice compared to control mice (Figure 1C-D). This latter result indicates that unlike ectopically administered rec N-Shh, endogenous endothelial Dhh prevents VEGFA-induced angiogenesis indicating that endothelial Dhh is rather anti-angiogenic. Importantly neither Shh nor Ihh expression was modified in ECs to compensate for Dhh deficiency (Figure 1E-G). Similar results were obtained when we quantified migration of cultured ECs. Indeed, while treatment with rec N-Shh protein promoted EC migration (Figure 1H), Dhh knockdown in ECs (Figure 1I) also increased cell migration (Figure 1J).

Altogether, this first set of data demonstrates for the first time that ectopic N-Shh and EC-derived endogenous Dhh induce opposite effects especially in ECs.

5.2. Endothelial Dhh promotes BBB integrity while Ectopic administration of N-Shh disrupts it.

To confirm that endothelial Dhh and ectopic N-Shh induce opposite effects on ECs, we compared their effect on endothelial barrier integrity. Consistent, with previous investigations [17,39], expression of both Cdh5 and Cldn5 was significantly diminished at the BBB of Dhh^{ECKO} mice compared to littermate controls (Figure 2A-D). This was associated with fibrinogen and albumin extravasation (Figure 2A-B, E-F), demonstrating abnormal BBB permeability. To investigate the effects of N-Shh, both N-Shh-encoding and control lentiviruses were administered locally in the brain cortex of wild-type mice (Figure 3A). As shown in Figure 3B-E, N-Shh significantly reduced Cdh5 expression at the BBB which was associated with increased albumin and fibrinogen extravasation. Consistent results were obtained in HUVECs in which both Dhh knockdown or treatment with recombinant N-Shh protein increased Cdh5 junction thickness indicating destabilization of adherens junctions (Supplemental Figure 1A-D). Additionally, these results were confirmed in mouse primary cultured brain ECs that were either prepared from Dhh^{ECKO} mice and littermate controls, or from WT mice

which were then treated with either recombinant N-Shh protein or BSA. As shown in Supplemental Figure 1E Dhh deficiency in brain ECs led to disorganized Cdh5 junctions and decreased expression of tight junction proteins including Cldn5 and Ocln (Supplemental Figure 1F-I). Treatment with rec N-Shh also altered brain EC junctions as it led to increased Cdh5 and Cldn5 internalization (Supplemental Figure 1J) and Cldn5 downregulation (Supplemental Figure 1K-N).
This second set of data confirms that endothelial Dhh and ectopic N-Shh trigger opposite effects: while endothelial Dhh promotes endothelium integrity, ectopic N-Shh destabilizes blood vessels.

5.3. Activating Smo mimics endothelial Dhh induced effects while inhibiting Smo recapitulates N-Shh effects

Since endothelial Dhh and ectopic N-Shh induce opposite effects in ECs, we hypothesized that one of the ligand would activate Hh signaling in EC while the other would inhibit it. To test this hypothesis, we assessed the functional consequences of Smo modulation since the classical readout to assess Hh signalling activity (i.e. Gli activity) is not modulated in ECs (Supplemental Figure 2). First, we investigated the role of endothelial Smo in angiogenesis; VEGFA containing pellets were implanted in the corneas of both Smo^{ECKO} mice and their control littermates. Interestingly, Smo deficiency significantly increased VEGFA-induced angiogenesis (Supplemental Figure 3A-B). Consistently, *in vitro*, Smo inhibition with GDC-0449 significantly stimulated HUVEC migration while Smo activation with the Smo agonist SAG did not (Supplemental Figure 3C). Then we investigated the role of Smo on endothelial barrier integrity; Smo deficiency in ECs significantly decreased both Cdh5 and Cldn5 expression at the BBB (Supplemental Figure 3 D-G), which was associated with increased fibrinogen and albumin extravasation (Supplemental Figure 3D-E and H-I). *In vitro*, GDC-0449 increased Cdh5 junction thickness in both HUVECs (Supplemental Figure 4A-B) and mouse brain EC (Supplemental Figure 4C). Moreover, it induced Cldn5 internalization in mouse brain EC (Supplemental Figure 4C). Besides, SAG increased Cldn5 expression in mouse brain EC (Supplemental Figure 4D-F).
Altogether these results suggest that Dhh activates Hh signalling in ECs via Smo while ectopic N-Shh inhibits it. In order to verify this hypothesis, we performed rescue experiments. ECs were either transfected with control or Dhh siRNA and then treated or not with SAG. As expected, the increased Cdh5 junction thickness observed in the absence of Dhh was reversed in the presence of SAG (Supplemental Figure 5A-B). In parallel, ECs were treated with rec N-Shh in the presence or not of SAG. Once again, N-Shh-induced increased Cdh5 junction thickness was reversed in the presence of SAG (Supplemental Figure 5C-D) suggesting that ectopic N-Shh inhibits Dhh-induced autocrine signalling in ECs.

5.4. Dhh promotes endothelium integrity under its 43 kDa full-length soluble form

With the aim to investigate why endothelial Dhh and ectopic N-Shh induce opposite effects in ECs, we first wished to characterize under which form endothelial Dhh promotes endothelial integrity. Notably, while Shh is mainly processed as a 19 kDa N-terminal peptide and secreted as both a 45 kDa full-length peptide and 19 kDa N-terminal peptide (Supplemental Figure 6A), Dhh is mainly produced as a 43 kDa full-length protein and secreted exclusively under this form (Supplemental Figure 6B).
We then tested whether Dhh requires being palmitoylated using the Hedgehog acyltransferase (HHAT) inhibitor RU-SKI 43. RU-SKI did not modulate neither HUVEC migration nor HUVEC junction thickness (Figure 4A-C), indicating that Dhh may not need to be palmitoylated to promote endothelium integrity. To investigate the role of Disp1, a transmembrane protein necessary for Hh ligand transport across the plasma membrane, HUVECs were transfected with Disp1 or control siRNA

(Figure 4D). Disp1 knockdown in HUVECs enhanced HUVEC migration (Figure 4E), increased Cdh5+ junction thickness (Figure 4F-G) and endothelium permeability (Figure 4H). Consistent with Dhh being exposed at the cell surface or secreted, Hh blocking antibodies increased Cdh5 junction thickness in HUVECs (Figure 4I-J). Finally, to investigate whether Dhh acts as a membrane bound protein or as a soluble secreted protein, we tested whether conditioned medium containing soluble 43 kDa Dhh would restore adherens junction integrity in Dhh siRNA transfected HUVECs. Soluble 43 kDa Dhh prevented both Dhh siRNA-induced Cdh5+ junction thickening (Figure 4K-L) and endothelial permeability (Figure 4M) demonstrating that Dhh promotes endothelial integrity as a soluble 43 kDa, full-lengh.

In the meantime, we compared the effects of conditioned medium of HeLa cells transfected with either FL-Dhh, N-Shh, FL-Shh or N-Dhh encoding plasmids on HUVEC barrier properties. The conditioned medium from HeLa cells transfected with both N-Shh and FL-Shh encoding plasmids increased Cdh5 junction thickness (Supplemental Figure 6C-D) and increased endothelial monolayer permeability (Supplemental Figure 6E) confirming recombinant N-Shh protein effects. Notably, 17 kDa N-Dhh containing conditioned medium recapitulated the effects of N-Shh but not these of FL-Dhh demonstrating that Dhh requires being under its 43 kDa full-length form to promote endothelium integrity and suggesting that any N-Hh ligands would inhibit Hh signalling in ECs.

5.5. N-Shh prevents FL-Dhh binding to Ptch1

We hypothesized that N-Hh ligands inhibit Hh signaling in ECs by preventing Dhh-induced signalling. First, we quantified Dhh binding to Ptch1 in the presence or absence of N-Shh. To do so, we verified that both 43 kDa Dhh and N-Shh bind Ptch1 in immunoprecipitation assays (Figure 5A-B). We then measured the amount of 43 kDa Dhh bound to Ptch1 in the presence or absence of N-Shh by immunoprecipitation assay. Dhh binding to Ptch1 was reduced by about 70-80% in the presence of N-Shh (Figure 5C-D). The same result was obtained in the proximity ligation assay (Figure 5E-F). Notably, N-Dhh also bound Ptch1 (Supplemental Figure 7A). However, N-Dhh prevented 43 kDa Dhh binding to Ptch1 to the same extent as N-Shh while FL-Shh only decreased 43 kDa Dhh binding to Ptch1 by 50% (Supplemental Figure 7B-C).

Altogether these results indicate for the first time that N-Hh ligands may act as competitive antagonists to 43 kDa Dhh in ECs.

5.6. Each forms of Hh ligands induces a specific localization in Ptch1

The key remaining question was to determine why N-Hh ligands are not recapitulating 43 kDa Dhh-induced effects once they bind Ptch1. Therefore, we decided to investigate the earliest signalling events following Hh ligands binding to Ptch1. Upon Hh ligands binding to Ptch1, Ptch1 is being internalized and degraded by the ubiquitin proteasome system [40]. Accordingly, FL-Dhh, N-Shh, N-Dhh and FL-Shh all induced Ptch1 degradation (Supplemental Figure 8A-B) and neither of them modulated 43 kDa FL-Dhh-induced Ptch1 degradation (Supplemental Figure 8C-D).

On the contrary, each Hh ligand and form of Hh ligand induced a distinct localization of Ptch1. 43 kDa Dhh provoked a peri-nuclear localization of Ptch1, FL-Shh triggered Ptch1 endocytosis into vesicle distributed within the entire cell, while N-Shh and N-Dhh induced the formation of big Ptch1 aggregates in cells (Supplemental Figure 8E). As a consequence, N-Shh prevented 43 kDa Dhh-induced massive peri-nuclear localization of Ptch1 (Figure 5G). Finally, we verified whether the same

was true in ECs, to this end, we repeated this last experiment in HUVECs. Consistently with results obtained in HeLa, N-Shh prevented 43 kDa Dhh-induced Ptch1 peri-nuclear localization (Figure 5H).

5.7. Astrocyte-derived Shh disrupts BBB in the setting of brain inflammation

Finally, since we have only been investigating the vascular effects of ectopic N-Shh so far, we wished to investigate whether such regulation of Hh signalling exists in pathophysiological settings. Interestingly, while, Shh is barely expressed in the healthy vasculature, its expression is strongly upregulated in perivascular astrocytes upon brain inflammation (Supplemental Figure 9B) [2]. More specifically, Shh mRNA is strongly up regulated in astrocytes upon Il-1β treatment (Supplemental Figure 9C) and we verified that Il1β-treated astrocytes produce a N-terminal fully processed Shh form (Supplemental Figure 9D). We then performed a series of experiments to investigate what would be the paracrine effects of astrocyte-derived Shh on endothelial barrier integrity. We compared BBB integrity in the setting of Il1β-induced acute inflammation in both mice deficient for Shh in astrocytes (Shh^{ACKO}) and in their control littermates. At 7 days after AdIl1β brain microinjection (Supplemental Figure 9E), expression of both Cdh5 and Cldn5 were significantly increased in the absence of astrocyte-derived Shh (Supplemental Figure 9F-H). This was associated with decreased extravasation of serum proteins including fibrinogen and albumin (Supplemental Figure 9I-K) demonstrating for the first time that astrocytic Shh expression disrupts BBB integrity during acute neuro-inflammation.

5.8. Mice with astrocyte Shh inactivation display reduced disability in a model of multiple sclerosis

To examine the impact of these findings on disease severity, we investigated the phenotype of the multiple sclerosis model (EAE) in Shh^{ACKO} and control mice. Mice were sensitized with the encephalitogenic myelin peptide $MOG_{35–55}$ and sacrificed 32 days later. Consistent with the acute cortex inflammation model, expression of both Cdh5 and Cldn5 were significantly increased at the endothelium of spinal cord vessels in the absence of astrocyte-derived Shh (Figure 6A-C). Accordingly, fibrinogen and albumin extravasation was reduced (Figure 6D-F). These results thus confirmed the damaging role of astrocytic Shh at the BBB. As a consequence, in the absence of astrocyte-derived Shh, leucocyte entry in the spinal cord parenchyma was reduced (Figure 7A-B), so was microglia (Figure 7C-D) and astrocyte activation (Figure 7E-F) which all together concur to prevent demyelination (Figure 7G-H). Finally, the clinical consequences of astrocytic Shh deficiency were evaluated using a widely accepted 5-point paradigm from day 7 until the end of the experiment at day 32 after sensitization (Figure 7I). Critically, these studies revealed that the clinical course and pathology of EAE were strongly reduced in Shh^{ACKO} mice during the plateau of the disease. In controls, neurologic deficit was observed from day 9, and increased in severity until day 29, when clinical score stabilized at a mean of 2,91, representing hind limb paralysis. In contrast, the onset of clinical signs in Shh^{ACKO} mice was first seen 3 days later, and the clinical course was much milder. In Shh^{ACKO} mice, disease reached a plateau at day 19 at a mean of 1,78, indicating hind limb weakness and unsteady gait, a mild phenotype, and this divergence in scores are significant from day 8 to day 32 after sensitization (Figure 7I). The peak EAE score (1.75 vs 2.86 in control mice), total average score (0.86 vs 1.20 in control mice), and score during the time of disability (1.31 vs 1.82 in control mice) were all decreased in Shh^{ACKO} mice (data not shown) but there were no significant changes in survival and mortality rates (data not shown).

In conclusion, this last set of data reveals for the first time that N-Shh may indeed act as a Dhh antagonist in a pathophysiological setting especially brain inflammation.

6. Discussion

While Hh ligands are typically used instead of another for therapeutic purposes [41], the present study is the first one to our knowledge reporting that each forms of Hh ligand may induce its own specific effects. As a consequence, Hh ligands can enter into competition between each other to induce their effects. Notably, this is not the first time that different form of Hh ligand were reported to compete between each other, indeed, more than 20 years ago, unpalmitoylated Hh ligands were reported to act as dominant inhibitors toward palmitoylated Shh by competing for Ptch1 binding [42]. These findings, together with our findings, thus highlight a totally new mode of Hh signalling regulation based on the regulation of Hh ligand processing.

More specifically, in this study, we have investigated the effects of Hh ligands on ECs and compared the autocrine effects of 43 kDa FL-Dhh to the paracrine effects of 19 kDa N-Shh. We found that 43 kDa FL-Dhh promotes endothelial barrier integrity and stabilizes blood vessels, while 19 kDa N-Shh destabilizes endothelial intercellular junctions and promotes angiogenesis at least in part by acting as a competitive inhibitor of 43 kDa FL-Dhh (Supplemental Figure 10) demonstrating that Hh ligands cannot be used instead of another for therapeutic purposes. Moreover, 17 kDa N-Dhh also acts as a competitive inhibitor of 43 kDa FL-Dhh demonstrating that the different form of Hh ligands can also not be used instead of another.

While canonical Hh signalling is typically induced in a “mesemchymal type” cell by a fully processed 19 kDa N-Shh form produced by an “epithelial like” cell, Hh signaling in ECs occurs through a non-canonical autocrine signalling. Consistent with the present finding, such signalling was shown to be induced by full-length unprocessed Hh ligands [43]. However the molecular mechanisms by which 43 kDa FL-Dhh promotes endothelial barrier function remains to be characterized. All that we know so far is that 43 kDa FL-Dhh-induced endothelial barrier integrity involves Smo but is more likely independent on Gli transcription factors. Besides, consistent with Taddei et al. results, Dhh regulation of Cldn5 depends on FoxO1 [27], suggesting that Smo does not regulate tight junctions directly but rather through the regulation of adherens junctions. To further characterize this pathway, it is critical to fully understand why 43 kDa FL-Dhh, 45 kDa FL-Shh, 17 kDa N-Dhh and 19 N-Shh do not all induce the same effects in ECs. Indeed, while they all induce Ptch1 degradation through the proteasome, each of them induces a specific Ptch1 re-localization. Notably, Ptch1 inhibition and internalization were shown to be carried out by separable parts of Shh [44], explaining why some Hh ligands-induced effects may be induced by any form of Hh ligands while other may be specific for one form or another. Consistently, it is currently not known why 19 kDa N-Shh is a strong activator of Gli1 transcription in fibroblast while 17 kDa N-Dhh is not [22].

Importantly, the present study may resolve quite a few inconsistent literature data regarding the role of Hh signalling in vascular biology [14]. Indeed, in most studies that have investigated Shh effect on angiogenesis, Shh was delivered ectopically under its N-terminal form and was shown to be pro-angiogenic [1,5,15] which is fully consistent with the results obtained in the present study. However, it would be necessary to determine the cell origin and the form under which endogenous Shh is produced in the setting of ischaemia to apprehend why ischaemia-induced angiogenesis was shown to be accelerated in Shh deficient mice [16]. Besides, studies reporting that Hh signalling promotes BBB integrity in adults have either used Smo inhibitors, Smo^{ECKO} or Dhh^{ECKO} mice [2,17,45]. In each of these cases, 43 kDa FL-Dhh-induced, Smo-dependent autocrine signalling in ECs was then more likely responsible for the findings. On the contrary, when glioblastoma-derived Dhh was shown to disrupt

the BBB [18], it may have been produced under its 17 kDa N-Dhh form which competes with 43 kDa FL-Dhh. The same conclusion can be made from the study reporting that ectopic Shh expression induces haemorrhage in the spinal cord [19]. Once again either FL-Shh or N-Shh may have acted as 43 kDa FL-Dhh competitive antagonists.
Moreover, while Hh signalling is mostly shown to be good for the cardiovascular system, Scube2 which was shown to be upregulated in the setting of type 2 diabetes [46] and atherosclerosis [47], has been associated with endothelial dysfunction [46] and has a strong proangiogenic activity [48,49]. Since Scube2 promotes soluble 19 kDa cholesterol-esterified N-Shh release, these results are actually fully consistent with the conclusion of the present study i.e. 43 kDa FL-Dhh promotes endothelial barrier integrity and inhibits angiogenesis while 19 kDa N-Shh destabilizes endothelial intercellular junctions and promotes angiogenesis.

In conclusion, the present study reveals unsuspected competitive and antagonistic activities of the different forms and types of Hh ligands in the adult cardiovascular systems especially ECs. Such results represent a breakthrough regarding our understanding of the regulation of Hh signaling and demonstrate that Hh ligands or form of Hh ligands cannot be used instead of another for therapeutic purposes.

7. Funding

This study was supported by grants from the Fondation de France (Appel d'Offre Recherche sur les maladies Cardiovasculaires 2013 and 2018), and the Fondation ARSEP pour la recherche sur la sclérose en plaques. Also this study was funded by a Marie Skłodowska-Curie Actions (MSCA-IF-2019) from the European council. Finally, this study was co-funded by the "Institut National de la Santé et de la Recherche Médicale" and by the University of Bordeaux.

8. Acknowledgments

We thank Annabel Reynaud, Sylvain Grolleau, and Maxime David for their technical help. We thank Christelle Boullé for administrative assistance.

9. Conflict of interest

None declared

10. References

1. Pola R, Ling LE, Silver M, Corbley MJ, Kearney M, Blake Pepinsky R, Shapiro R, Taylor FR, Baker DP, Asahara T, Isner JM. The morphogen Sonic hedgehog is an indirect angiogenic agent upregulating two families of angiogenic growth factors. *Nat Med* 2001;**7**:706–711.

2. Alvarez JI, Dodelet-Devillers A, Kebir H, Ifergan I, Fabre PJ, Terouz S, Sabbagh M, Wosik K, Bourbonniere L, Bernard M, Horssen J van, Vries HE de, Charron F, Prat A. The Hedgehog pathway promotes blood-brain barrier integrity and CNS immune quiescence. *Science* 2011;**334**:1727–1731.

3. Pola R, Ling LE, Aprahamian TR, Barban E, Bosch-Marce M, Curry C, Corbley M, Kearney M, Isner JM, Losordo DW. Postnatal recapitulation of embryonic hedgehog pathway in response to skeletal muscle ischemia. *Circulation* 2003;**108**:479–485.

4. Lavine KJ, Kovacs A, Ornitz DM. Hedgehog signaling is critical for maintenance of the adult coronary vasculature in mice. *J Clin Invest* 2008;**118**:2404–2414.

5. Kusano KF, Pola R, Murayama T, Curry C, Kawamoto A, Iwakura A, Shintani S, Ii M, Asai J, Tkebuchava T, Thorne T, Takenaka H, Aikawa R, Goukassian D, Samson P von, Hamada H, Yoon YS, Silver M, Eaton E, Ma H, Heyd L, Kearney M, Munger W, Porter JA, Kishore R, Losordo DW. Sonic hedgehog myocardial gene therapy: tissue repair through transient reconstitution of embryonic signaling. *Nat Med* 2005;**11**:1197–1204.

6. Xia YP, He QW, Li YN, Chen SC, Huang M, Wang Y, Gao Y, Huang Y, Wang MD, Mao L, Hu B. Recombinant human sonic hedgehog protein regulates the expression of ZO-1 and occludin by activating angiopoietin-1 in stroke damage. *PLoS One* 2013;**8**:e68891.

7. Chapouly C, Yao Q, Vandierdonck S, Larrieu-Lahargue F, Mariani JN, Gadeau AP, Renault MA. Impaired Hedgehog signalling-induced endothelial dysfunction is sufficient to induce neuropathy: implication in diabetes. *Cardiovasc Res* 2016;**109**:217–227.

8. Lavine KJ, Ornitz DM. Rebuilding the coronary vasculature: hedgehog as a new candidate for pharmacologic revascularization. *Trends Cardiovasc Med* 2007;**17**:77–83.

9. Cristofaro B, Emanueli C. Possible novel targets for therapeutic angiogenesis. *Curr Opin Pharmacol* 2009;**9**:102–108.

10. Pan JY, Zhou SH. The hedgehog signaling pathway, a new therapeutic target for treatment of ischemic heart disease. *Pharm* 2012;**67**:475–481.

11. Wang Y, Lu P, Zhao D, Sheng J. Targeting the hedgehog signaling pathway for cardiac repair and regeneration. *Herz* 2017;**42**:662–668.

12. Dunaeva M, Waltenberger J. Hh signaling in regeneration of the ischemic heart. *Cell Mol Life Sci CMLS* 2017;**74**:3481–3490.

13. Salybekov AA, Salybekova AK, Pola R, Asahara T. Sonic Hedgehog Signaling Pathway in Endothelial Progenitor Cell Biology for Vascular Medicine. *Int J Mol Sci* 2018;**19**.

14. Chapouly C, Guimbal S, Hollier P-L, Renault M-A. Role of Hedgehog Signaling in Vasculature Development, Differentiation, and Maintenance. *Int J Mol Sci* 2019;**20**.

15. Renault MA, Roncalli J, Tongers J, Thorne T, Klyachko E, Misener S, Volpert OV, Mehta S, Burg A, Luedemann C, Qin G, Kishore R, Losordo DW. Sonic hedgehog induces angiogenesis via Rho kinase-dependent signaling in endothelial cells. *J Mol Cell Cardiol* 2010;**49**:490–498.

16. Caradu C, Guy A, James C, Reynaud A, Gadeau AP, Renault MA. Endogenous Sonic Hedgehog limits inflammation and angiogenesis in the ischemic skeletal muscle of mice. *Cardiovasc Res* 2018;

17. Caradu C, Couffinhal T, Chapouly C, Guimbal S, Hollier P-L, Ducasse E, Bura-Rivière A, Dubois M, Gadeau A-P, Renault M-A. Restoring Endothelial Function by Targeting Desert Hedgehog Downstream of Klf2 Improves Critical Limb Ischemia in Adults. *Circ Res* 2018;**123**:1053–1065.

18. Azzi S, Treps L, Leclair HM, Ngo H-M, Harford-Wright E, Gavard J. Desert Hedgehog/Patch2 Axis Contributes to Vascular Permeability and Angiogenesis in Glioblastoma. *Front Pharmacol* 2015;**6**:281.

19. Rowitch DH, S. Jacques B, Lee SM, Flax JD, Snyder EY, McMahon AP. Sonic hedgehog regulates proliferation and inhibits differentiation of CNS precursor cells. *J Neurosci* 1999;**19**:8954–8965.

20. Nusslein-Volhard C, Wieschaus E. Mutations affecting segment number and polarity in Drosophila. *Nature* 1980;**287**:795–801.

21. Robbins DJ, Fei DL, Riobo NA. The Hedgehog signal transduction network. *Sci Signal* 2012;**5**:re6.

22. Pathi S, Pagan-Westphal S, Baker DP, Garber EA, Rayhorn P, Bumcrot D, Tabin CJ, Blake Pepinsky R, Williams KP. Comparative biological responses to human Sonic, Indian, and Desert hedgehog. *Mech Dev* 2001;**106**:107–117.

23. Chinchilla P, Xiao L, Kazanietz MG, Riobo NA. Hedgehog proteins activate pro-angiogenic responses in endothelial cells through non-canonical signaling pathways. *Cell Cycle* 2010;**9**:570–579.

24. Farzan SF, Singh S, Schilling NS, Robbins DJ. Hedgehog Processing and Biological Activity. *Am J Physiol Gastrointest Liver Physiol* 2008;**294**:G844–G849.

25. Tukachinsky H, Kuzmickas RP, Jao CY, Liu J, Salic A. Dispatched and scube mediate the efficient secretion of the cholesterol-modified hedgehog ligand. *Cell Rep* 2012;**2**:308–320.

26. Pettigrew CA, Asp E, Emerson CP. A new role for Hedgehogs in juxtacrine signaling. *Mech Dev* 2013;**131**:137–149.

27. Hollier P-L, Guimbal S, Mora P, Diop A, Cornuault L, Couffinhal T, Gadeau A-P, Renault M-A, Chapouly C. Genetic disruption of the Blood Brain Barrier leads to protective barrier formation at the Glia Limitans. *bioRxiv* Cold Spring Harbor Laboratory; 2020;2020.03.13.990762.

28. Lehmann GL, Hanke-Gogokhia C, Hu Y, Bareja R, Salfati Z, Ginsberg M, Nolan DJ, Mendez-Huergo SP, Dalotto-Moreno T, Wojcinski A, Ochoa F, Zeng S, Cerliani JP, Panagis L, Zager PJ, Mullins RF, Ogura S, Lutty GA, Bang J, Zippin JH, Romano C, Rabinovich GA, Elemento O, Joyner AL, Rafii S, Rodriguez-Boulan E, Benedicto I. Single-cell profiling reveals an endothelium-mediated immunomodulatory pathway in the eye choroid. *J Exp Med* 2020;**217**.

29. Dakubo GD, Mazerolle C, Furimsky M, Yu C, St-Jacques B, McMahon AP, Wallace VA. Indian hedgehog signaling from endothelial cells is required for sclera and retinal pigment epithelium development in the mouse eye. *Dev Biol* 2008;**320**:242–255.

30. Dassule HR, Lewis P, Bei M, Maas R, McMahon AP. Sonic hedgehog regulates growth and morphogenesis of the tooth. *Development* 2000;**127**:4775–4785.

31. Long F, Zhang XM, Karp S, Yang Y, McMahon AP. Genetic manipulation of hedgehog signaling in the endochondral skeleton reveals a direct role in the regulation of chondrocyte proliferation. *Development* 2001;**128**:5099–5108.

32. Melo J de, Miki K, Rattner A, Smallwood P, Zibetti C, Hirokawa K, Monuki ES, Campochiaro PA, Blackshaw S. Injury-independent induction of reactive gliosis in retina by loss of function of the LIM homeodomain transcription factor Lhx2. *Proc Natl Acad Sci U S A* 2012;**109**:4657–4662.

33. Muzumdar MD, Tasic B, Miyamichi K, Li L, Luo L. A global double-fluorescent Cre reporter mouse. *Genesis* 2007;**45**:593–605.

34. Azzoni E, Conti V, Campana L, Dellavalle A, Adams RH, Cossu G, Brunelli S. Hemogenic endothelium generates mesoangioblasts that contribute to several mesodermal lineages in vivo. *Development* 2014;**141**:1821–1834.

35. Caradu C, Couffinhal T, Chapouly C, Guimbal S, Hollier P-L, Ducasse E, Bura-Rivière A, Dubois M, Gadeau A-P, Renault M-A. Restoring Endothelial Function by Targeting Desert Hedgehog Downstream of Klf2 Improves Critical Limb Ischemia in Adults. *Circ Res* 2018;**123**:1053–1065.

36. Kenyon BM, Voest EE, Chen CC, Flynn E, Folkman J, D'Amato RJ. A model of angiogenesis in the mouse cornea. *Invest Ophthalmol Vis Sci* 1996;**37**:1625–1632.

37. Horng S, Therattil A, Moyon S, Gordon A, Kim K, Argaw AT, Hara Y, Mariani JN, Sawai S, Flodby P, Crandall ED, Borok Z, Sofroniew MV, Chapouly C, John GR. Astrocytic tight junctions control inflammatory CNS lesion pathogenesis. *J Clin Invest* 2017;**127**:3136–3151.

38. Argaw AT, Gurfein BT, Zhang Y, Zameer A, John GR. VEGF-mediated disruption of endothelial CLN-5 promotes blood-brain barrier breakdown. *Proc Natl Acad Sci U S A* 2009;**106**:1977–1982.

39. Chapouly C, Yao Q, Vandierdonck S, Larrieu-Lahargue F, Mariani JN, Gadeau AP, Renault MA. Impaired Hedgehog signalling-induced endothelial dysfunction is sufficient to induce neuropathy: implication in diabetes. *Cardiovasc Res* 2016;**109**:217–227.

40. Chen XL, Chinchilla P, Fombonne J, Ho L, Guix C, Keen JH, Mehlen P, Riobo NA. Patched-1 proapoptotic activity is downregulated by modification of K1413 by the E3 ubiquitin-protein ligase Itchy homolog. *Mol Cell Biol* 2014;**34**:3855–3866.

41. Calcutt NA, Allendoerfer KL, Mizisin AP, Middlemas A, Freshwater JD, Burgers M, Ranciato R, Delcroix JD, Taylor FR, Shapiro R, Strauch K, Dudek H, Engber TM, Galdes A, Rubin LL, Tomlinson DR. Therapeutic efficacy of sonic hedgehog protein in experimental diabetic neuropathy. *J Clin Invest* 2003;**111**:507–514.

42. Williams KP, Rayhorn P, Chi-Rosso G, Garber EA, Strauch KL, Horan GS, Reilly JO, Baker DP, Taylor FR, Koteliansky V, Pepinsky RB. Functional antagonists of sonic hedgehog reveal the importance of the N terminus for activity. *J Cell Sci* 1999;**112 (Pt 23)**:4405–4414.

43. Casillas C, Roelink H. Gain-of-function Shh mutants activate Smo cell-autonomously independent of Ptch1/2 function. *Mech Dev* 2018;**153**:30–41.

44. Tukachinsky H, Petrov K, Watanabe M, Salic A. Mechanism of inhibition of the tumor suppressor Patched by Sonic Hedgehog. *Proc Natl Acad Sci U S A* 2016;**113**:E5866–E5875.

45. Li T, Zhang J, Liu RY, Lian ZG, Chen XL, Ma L, Sun HM, Zhao YL. The role of the sonic hedgehog signaling pathway in early brain injury after experimental subarachnoid hemorrhage in rats. *Neurosci Lett* 2013;**552**:81–86.

46. Ali H, Rustam R, Aprilia D, Arizal C, Gusadri IB, Utami PR. Upregulation of SCUBE2 expression in dyslipidemic type 2 diabetes mellitus is associated with endothelin-1. *Diabetes Metab Syndr* 2019;**13**:2869–2872.

47. Ali H, Emoto N, Yagi K, Vignon-Zellweger N, Nakayama K, Hatakeyama K, Asada Y, Rikitake Y, Hirata K-I. Localization and characterization of a novel secreted protein, SCUBE2, in the development and progression of atherosclerosis. *Kobe J Med Sci* 2013;**59**:E122-131.

48. Lin Y-C, Chao T-Y, Yeh C-T, Roffler SR, Kannagi R, Yang R-B. Endothelial SCUBE2 Interacts With VEGFR2 and Regulates VEGF-Induced Angiogenesis. *Arterioscler Thromb Vasc Biol* 2017;**37**:144–155.

49. Lin Y-C, Liu C-Y, Kannagi R, Yang R-B. Inhibition of Endothelial SCUBE2 (Signal Peptide-CUB-EGF Domain-Containing Protein 2), a Novel VEGFR2 (Vascular Endothelial Growth Factor Receptor 2) Coreceptor, Suppresses Tumor Angiogenesis. *Arterioscler Thromb Vasc Biol* 2018;**38**:1202–1215.

Figures and Legend to Figures

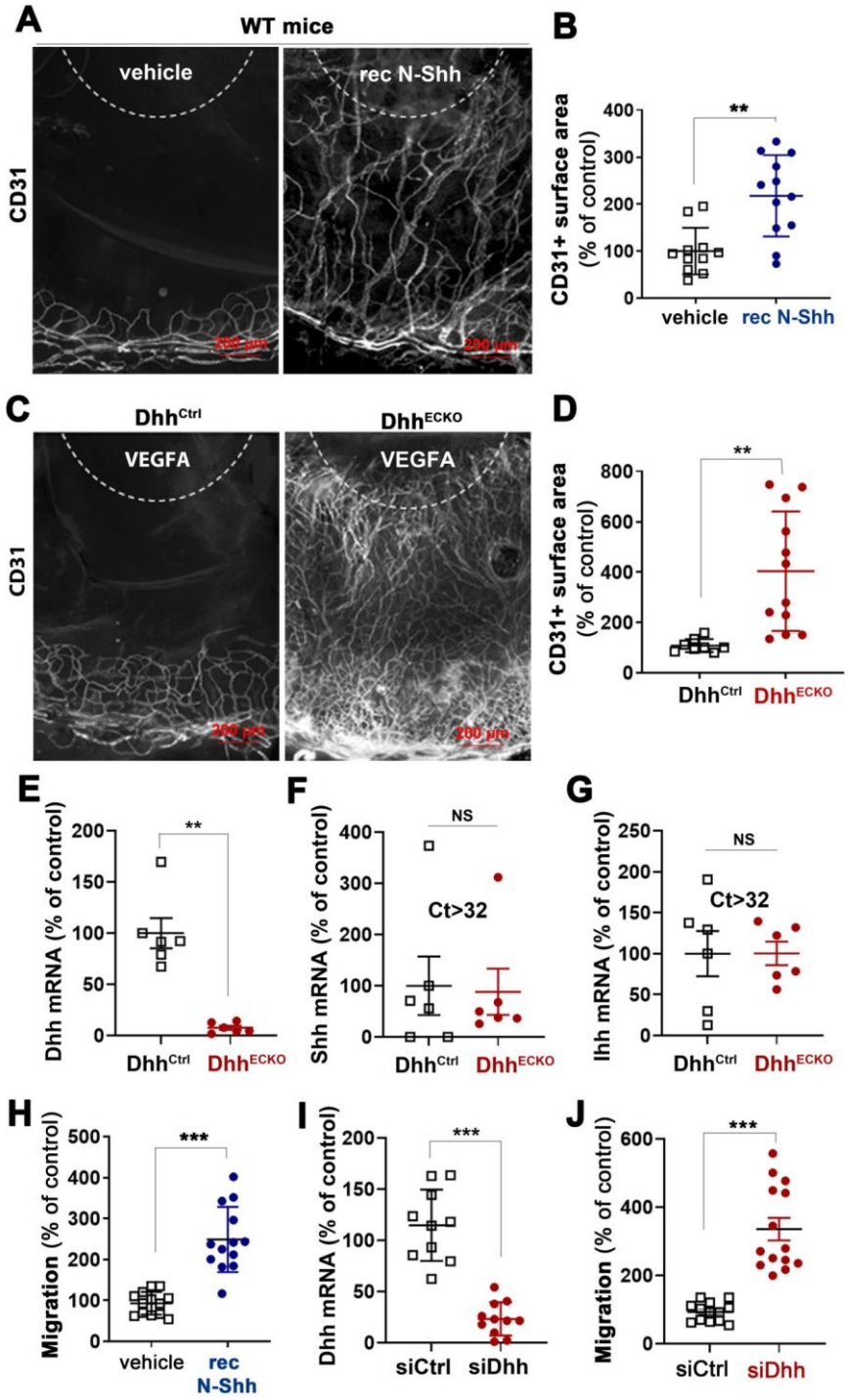

Figure 1: ***N-Shh promotes angiogenesis while EC-derived Dhh inhibits it.*** (**A-B**) recombinant N-Shh-containing or control pellets were implanted in the corneas of WT mice. Mice were sacrificed 9 days later. (**A**) Whole mount corneas were immunostained with anti-CD31 antibodies to identify blood vessels. Representative pictures are shown. (**B**) Angiogenesis was quantified as the percentage of CD31+ surface area (n=12 and 11 corneas respectively). (**C-G)** Cdh5-Cre^{ERT2} Dhh$^{Flox/Flox}$ (Dhh^{ECKO}) and Dhh$^{Flox/Flox}$ (Dhh^{Ctrl}) mice were administered with tamoxifen and sacrificed 2 weeks later. (**C-D**) VEGFA containing pellets were implanted in the corneas of Cdh5-Cre^{ERT2} Dhh$^{Flox/Flox}$ (Dhh^{ECKO}) and Dhh$^{Flox/Flox}$ (Dhh^{Ctrl}) mice 2 week after they were administered with tamoxifen. (**C**) Whole mount corneas were

immunostained with anti-CD31 antibodies to identify blood vessels. Representative pictures are shown. (**D**) Angiogenesis was quantified as the percentage of CD31+ surface area (n=12 and 8 corneas respectively). (**E**) Dhh, (**F**) Shh and (**G**) Ihh mRNA expression was quantified via RT-qPCR in ECs isolated from their brain (n=8 and n=6 in each group respectively). (**H**) HUVEC migration was assessed in a chemotaxis chamber in the presence or not of 1 µg/mL recombinant N-Shh (n=13 in each condition). (**I-J**) HUVECs were transfected with Dhh or control siRNAs. (**I**) Dhh mRNA was quantified via RT-qPCR (n=11 and 10 in each condition respectively). (**J**) Cell migration was assessed in a chemotaxis chamber (n=14 and 12 in each condition respectively). **: $p \leq 0.01$; ***: $p \leq 0.001$; NS: not significant. Mann-Whitney test.

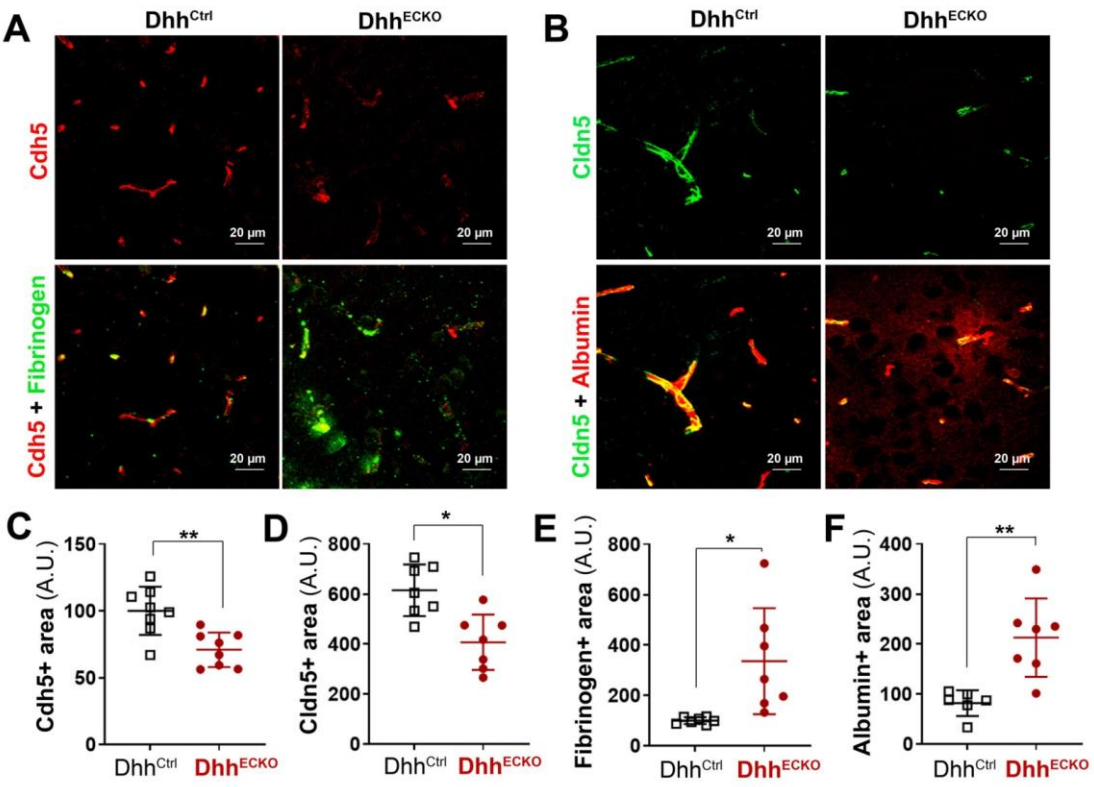

Figure 2: ***EC-derived Dhh prevents BBB opening while N-Shh disrupts it.*** Cdh5-Cre^{ERT2} Dhh$^{Flox/Flox}$ (Dhh^{ECKO}) and Dhh$^{Flox/Flox}$ (Dhh^{Ctrl}) mice were sacrificed 2 weeks after they were administered with tamoxifen. (**A-B**) Brain sagittal sections were immunostained with either anti-Cdh5 (in red), and anti-Fibrinogen (in green) antibodies (**A**) or anti-Cldn5 (in green) and anti-Albumin (in red) antibodies (**B**). Representative confocal images are shown. (**C**) Cdh5 expression was quantified as the Cdh5+ surface area (n=8 mice in each group). (**D**) Cldn5 expression was quantified as the Cldn5+ surface area (n=7 mice in each group). (**E**) Fibrinogen extravasation was quantified as the fibrinogen+ surface area (n=7 mice in each group). (**F**) Albumin extravasation was quantified as the albumin+ surface area (n=7 and 6 mice in each group respectively). *: p≤0.05; **: p≤0.01. Mann-Whitney test.

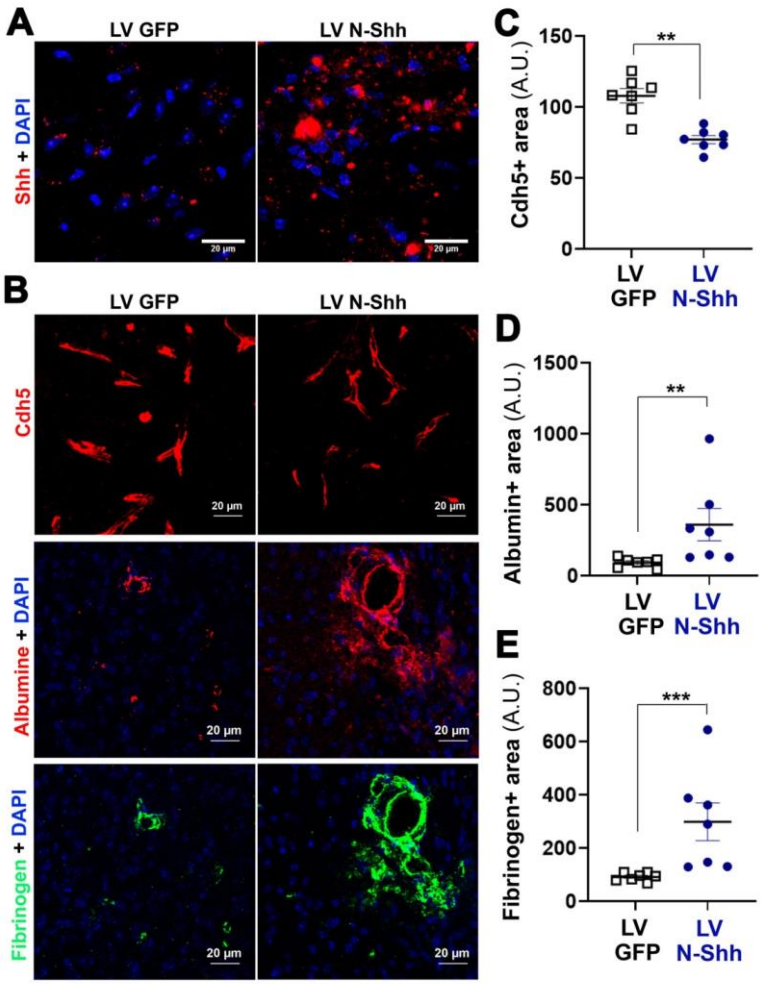

Figure 3: WT mice were administered in the cerebral cortex with lentiviruses encoding N-Shh (LV N-Shh) or not (LV GFP) (n= 7 mice in each group). Mice were sacrificed 14 days later. (**A**) Brain coronal sections were immunostained with anti-Shh antibodies (in red). (**B**) Brain coronal sections, chosen at the injection site, were immunostained with anti-Cdh5 (in red), anti-Albumin (in red) or anti-Fibrinogen (in green) antibodies. Representative confocal images are shown. (**C**) Cdh5 expression was quantified as the Cdh5+ surface area. (**D**) Albumin extravasation was quantified as the albumin+ surface area. (**E**) Fibrinogen extravasation was quantified as the fibrinogen+ surface area. **: p≤0.01; ***: p≤0.001. Mann-Whitney test.

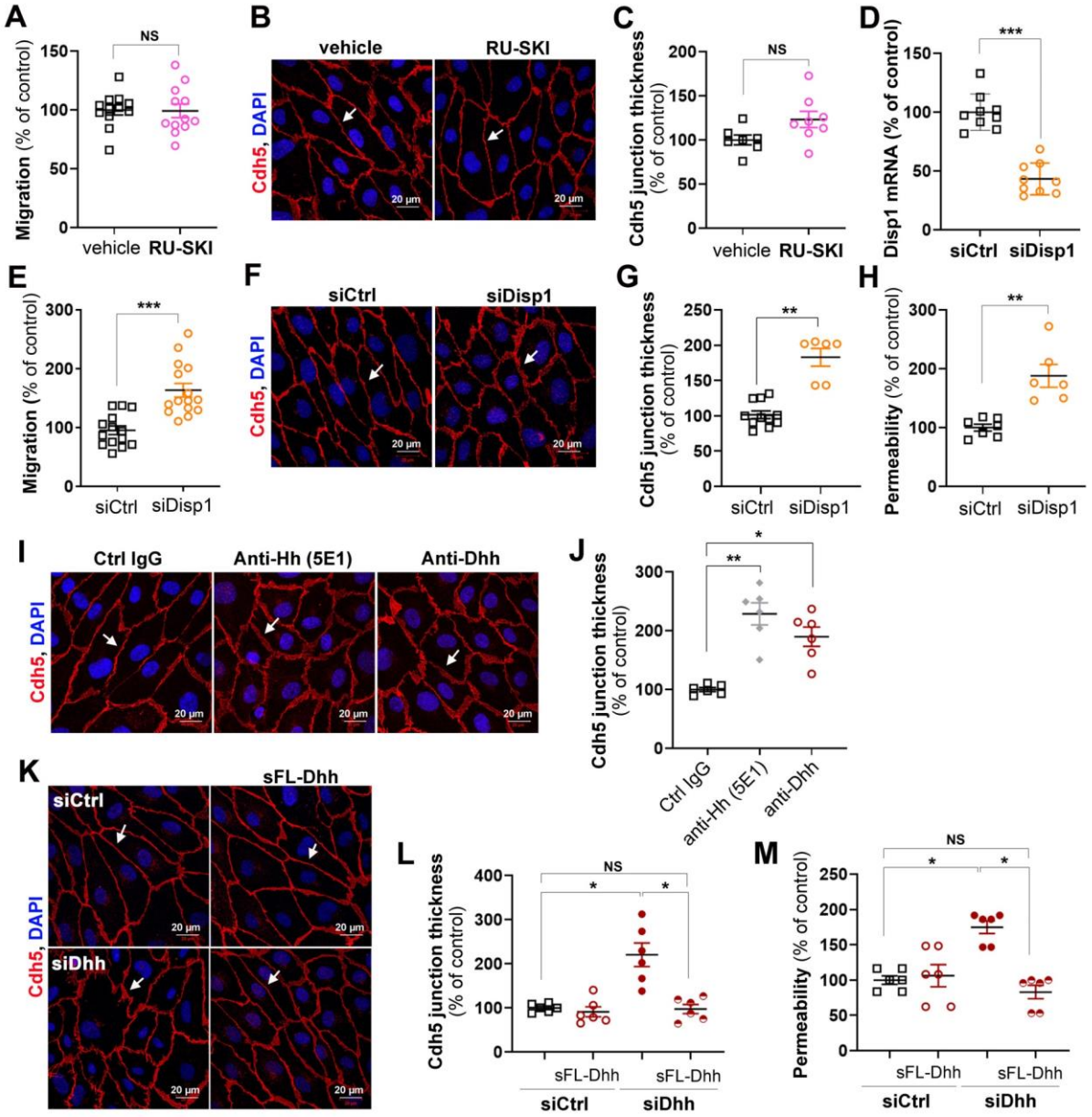

Figure 4: ***Dhh promotes endothelium integrity under its soluble form*****.** (**A-C**) HUVECs were treated or not with 10 µmol/L RU-SKI 43 (Sigma-Aldrich). (**A**) Cell migration was assessed in a chemotaxis chamber. The experiment was repeated 3 times, each experiment included n=4 wells/conditions. (**B**) Cdh5 localization was evaluated by immunofluorescent staining (in red) of a confluent cell monolayer and (**C**) quantified as the mean junction thickness using Image J software. The experiment was repeated 8 times. (**D-H**) HUVECs were transfected with Disp1 or control siRNAs. (**D**) Disp1 mRNA was quantified via RT-qPCR. The experiment was repeated 3 times, each experiment included n=3. (**E**) Cell migration was assessed in a chemotaxis chamber. The experiment was repeated 3 times, each experiment included n=4 wells/conditions. (**F**) Cdh5 localization was evaluated by immunofluorescent staining (in red) of a confluent cell monolayer and (**G**) quantified as the mean junction thickness using Image J software. The experiment was repeated 6 times. (**H**) Endothelial monolayer permeability to 70 kDa FITC-dextran was assessed using Transwells. The experiment was repeated 3 times, each experiment included duplicates. (**I-J**) HUVECs were treated either with 2 µg/mL Hh blocking antibodies (5E1, DSHB), 2 µg/mL Dhh blocking antibodies (Santa-Cruz

Biotechnology, sc271168), or 2 µg non-blocking mouse IgGs. (**I**) Cdh5 localization was evaluated by immunofluorescent staining (in red) of a confluent cell monolayer and (**J**) quantified as the mean junction thickness using Image J software. The experiment was repeated 6 times. (**K-M**) HUVECs were transfected with Dhh or control siRNAs, then treated with HeLa conditioned medium containing or not soluble FL-Dhh (sFL-Dhh). (**K**) Cdh5 localization was evaluated by immunofluorescent staining (in red) of a confluent cell monolayer and (**L**) quantified as the mean junction thickness using Image J software. The experiment was repeated 6 times. (**M**) Endothelial monolayer permeability to 70 kDa FITC-dextran was assessed using Transwells. The experiment was repeated 3 times, each experiment included duplicates. *: $p \leq 0.05$; **: $p \leq 0.01$; ***: $p \leq 0.001$; NS: not significant. Mann-Whitney test or Kruskal-Wallis test followed by Dunn's multiple comparison test.

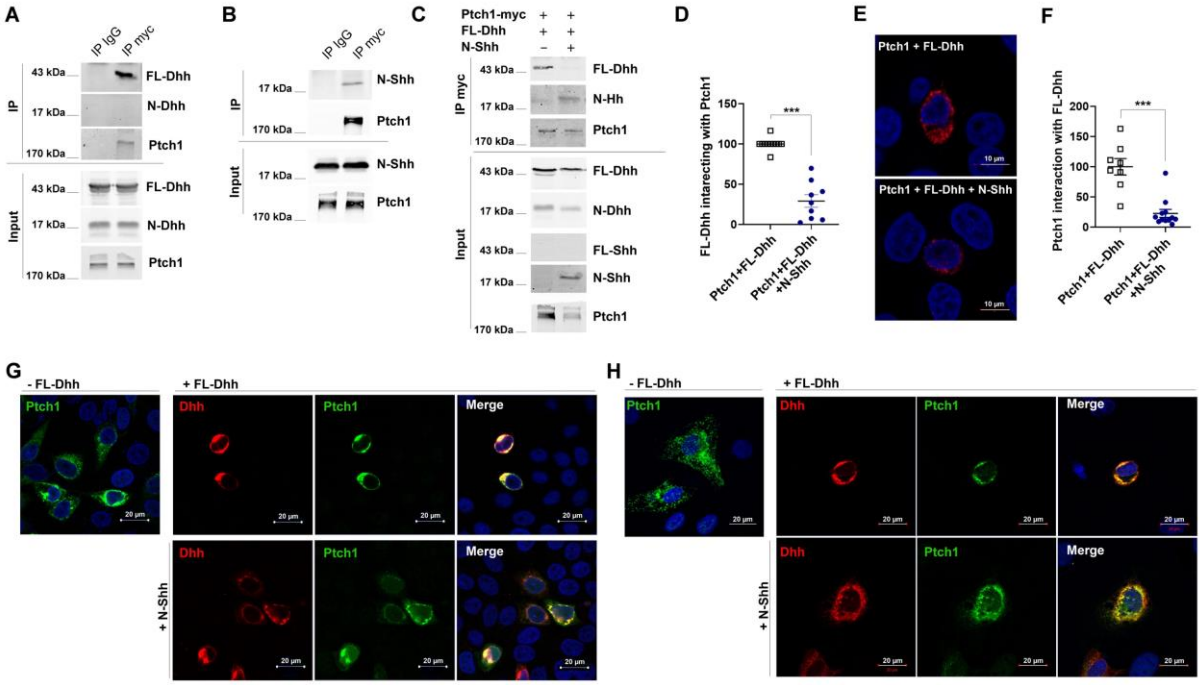

Figure 5: ***N-Shh prevents FL-Dhh binding to Ptch1*****.** (**A**) HeLa cells were co-transfected with Ptch1-myc and FL-Dhh encoding plasmids. Dhh interaction with Ptch1 was assessed by co-immunoprecipitation assay. (**B**) HeLa cells were co-transfected Ptch1-myc and N-Shh encoding plasmids. Dhh interaction with Ptch1 was assessed by co-immunoprecipitation assay. (**C-F**) HeLa cells were co-transfected Ptch1-myc and FL-Dhh encoding plasmids together with or without N-Shh encoding plasmids. (**C**) Dhh interaction with Ptch1 was assessed by co-immunoprecipitation assay and (**D**) quantified using Image J software. The experiment was repeated 9 times. (**E**) Dhh interaction with Ptch1 was assessed by proximity ligation assay and (**F**) quantified as mean red staining intensity/cell. Quantification were performed in 4 independent experiments. (**G**) Ptch1 and Dhh localization was assessed by immunostaining. (**H**) HUVECs were co-transfected with Ptch1-myc and FL-Dhh encoding plasmids together with or without N-Shh encoding plasmids. Ptch1 and Dhh localization were assessed by immunostaining. ***: p≤0.001; Mann-Whitney test.

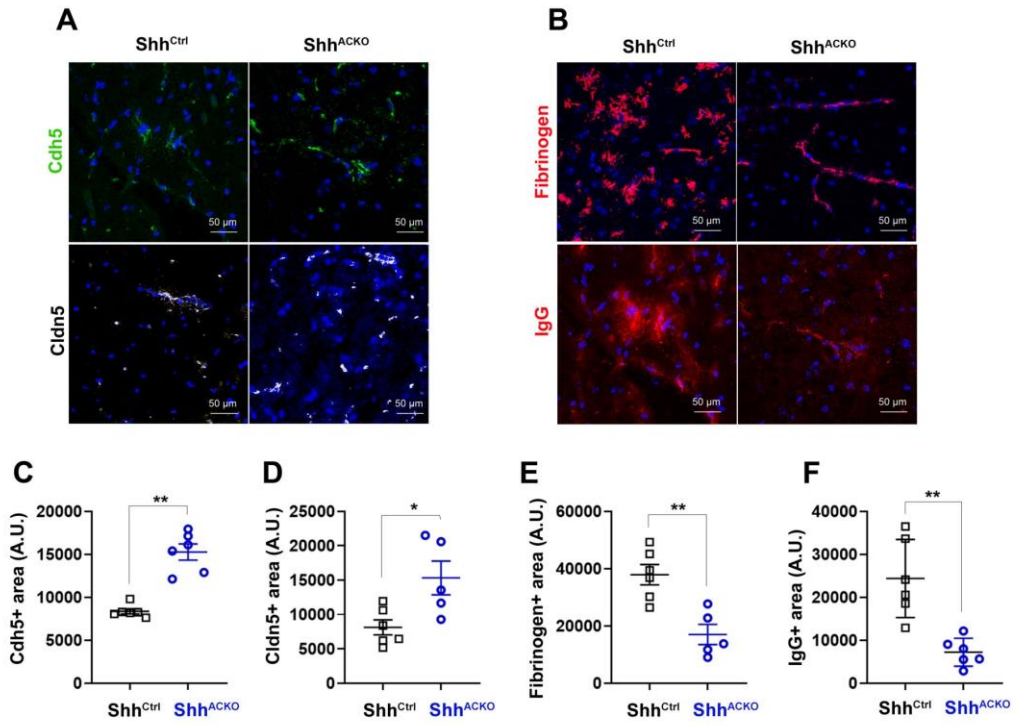

Figure 6: ***Astrocyte-derived Shh promotes BBB opening in the setting of CNS inflammation***
EAE was induced in both Shh^{ACKO} and Shh^{ctrl} mice (n=6 mice in each group). Mice were sacrificed 32 days later. (**A**) Spinal cord sections were immunostained with anti-Cdh5 (in green) and anti-Cldn5 (in white) antibodies. Representative confocal images are shown. Cdh5 (**B**) and Cldn5 (**C**) expression was quantified as the Cdh5+ (n=6 mice in each group) and Cldn5+ (n=6 and 5 mice in each group respectively) surface area respectively. (**D**) Spinal cord sections were immunostained with anti-Fibrinogen (in red) and anti-IgG (in red) antibodies. Representative confocal images are shown. Fibrinogen (**E**) and IgG (**F**) extravasation was quantified as the Fibrinogen+ (n=6 and 5 mice in each group respectively) surface area and IgG+ (n=6 mice in each group) surface area respectively. *: p≤0.05; **: p≤0.01. Mann-Whitney test.

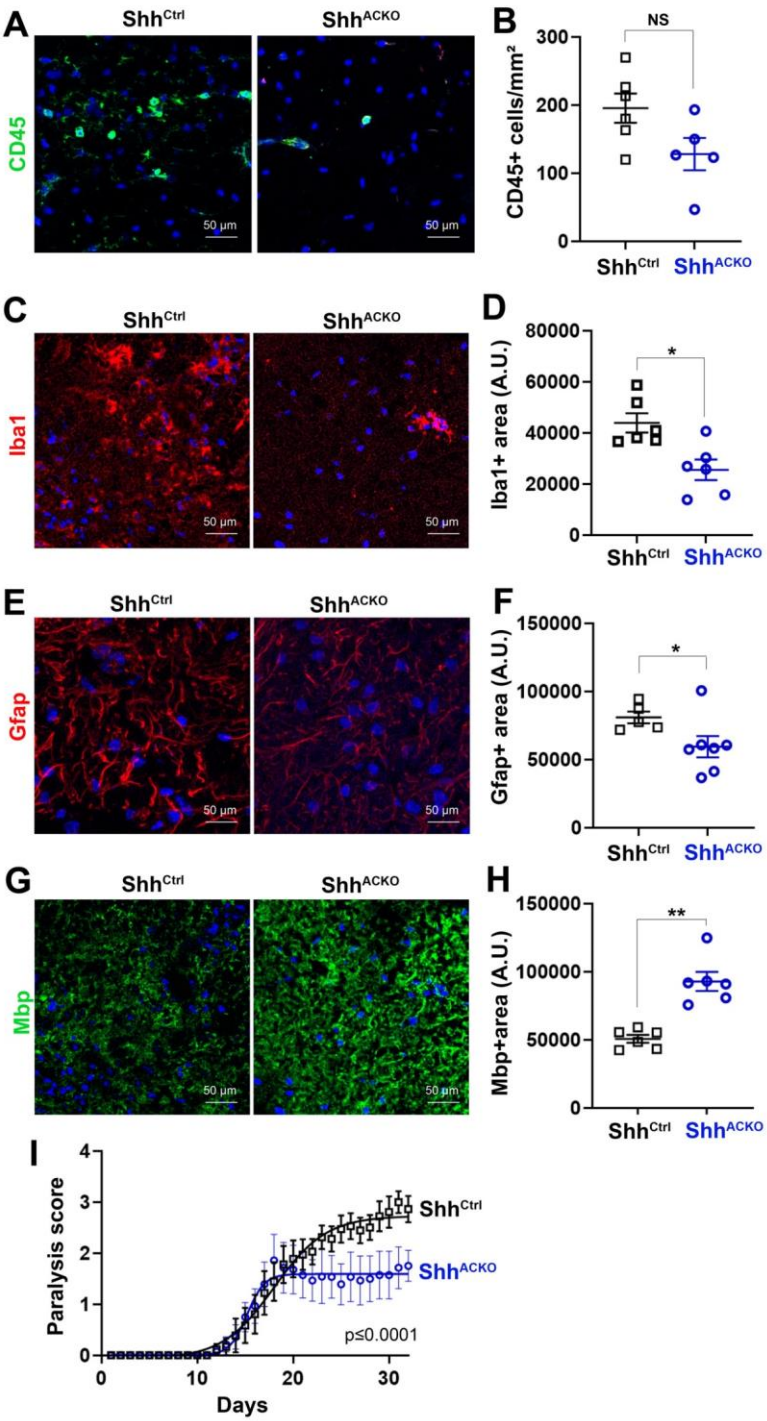

Figure 7: ***Astrocyte-derived Shh exacerbate EAE lesion formation and disease severity.*** EAE was induced in both Glast-Cre^{ERT2}; Shh$^{Flox/Flox}$ (Shh^{ACKO}) and Shh$^{Flox/Flox}$ (Shh^{ctrl}) mice (n=6 mice in each group). (**A-H**) Mice were sacrificed 32 days later. (**A**) Spinal cord cross sections were immunostained with anti-CD45 antibodies to identify leucocytes. Representative confocal images are shown. (**B**) Leucocyte infiltration was quantified as the number of CD45+cells/mm². (**C**) Spinal cord cross sections were immunostained with anti-Iba1 antibodies to identify microglia. Representative confocal images are shown. (**D**) Microglia activation was quantified as the Iba1+ surface area. (**E**) Activated Astrocytes were visualized after GFAP staining of Spinal cord cross sections. (**F**) Astrocyte activation was quantified as the Gfap+ surface area. (**G**) Spinal cord cross sections were immunostained with anti-

Mbp antibodies to identify myelin. (**H**) Myelination was quantified as the MBP+ surface area. (**I**) Mice were scored daily from day 7 until the end of the experiment at day 32 after sensitization on a standard 5-point scale, nonlinear regression (Boltzmann sigmoidal). *: p≤0.05; **: p≤0.01; NS: not significant; Mann-Whitney test.